

Journal of Biomedical Optics

BiomedicalOptics.SPIEDigitalLibrary.org

***In vivo* deep tissue imaging using wavefront shaping optical coherence tomography**

Hyeonseung Yu
Peter Lee
KyeoReh Lee
Jaeduck Jang
Jaeguyn Lim
Wooyoung Jang
Yong Jeong
YongKeun Park

In vivo deep tissue imaging using wavefront shaping optical coherence tomography

Hyeonseung Yu,^{a,b,†} Peter Lee,^{b,c,†} KyeoReh Lee,^{a,b} Jaeduck Jang,^d Jaeguyn Lim,^e Wooyoung Jang,^e Yong Jeong,^{b,c,*} and YongKeun Park^{a,b,f,*}

^aKorea Advanced Institute of Science and Technology, Department of Physics, Daejeon 34141, Republic of Korea
^bKI for optical Science and Technology, Daejeon 34141, Republic of Korea

^cKorea Advanced Institute of Science and Technology, Department of Bio and Brain Engineering, Daejeon 34141, Republic of Korea

^dSamsung Advanced Institute of Technology, Suwon, Gyeonggi 16678, Republic of Korea

^eSamsung Electronics, Suwon, Gyeonggi 16677, Republic of Korea

^fTomocube, Inc., Daejeon 34051, Republic of Korea

Abstract. Multiple light scattering in tissue limits the penetration of optical coherence tomography (OCT) imaging. Here, we present *in vivo* OCT imaging of a live mouse using wavefront shaping (WS) to enhance the penetration depth. A digital micromirror device was used in a spectral-domain OCT system for complex WS of an incident beam which resulted in the optimal delivery of light energy into deep tissue. *Ex vivo* imaging of chicken breasts and mouse ear tissues showed enhancements in the strength of the image signals and the penetration depth, and *in vivo* imaging of the tail of a live mouse provided a multilayered structure inside the tissue. © The Authors. Published by SPIE under a Creative Commons Attribution 3.0 Unported License. Distribution or reproduction of this work in whole or in part requires full attribution of the original publication, including its DOI. [DOI: [10.1117/1.JBO.21.10.101406](https://doi.org/10.1117/1.JBO.21.10.101406)]

Keywords: optical coherence tomography; imaging through turbid media; *in vivo* imaging.

Paper 150724LSSRR received Oct. 27, 2015; accepted for publication Jan. 25, 2016; published online Feb. 19, 2016.

Optical coherence tomography (OCT) provides noninvasive imaging of biological tissues based on low-coherence interferometry.¹ Analogous to ultrasound imaging, the use of infrared wavelengths in OCT provides a micrometer resolution and has been successfully used in various applications, particularly in ophthalmology. However, when imaging general tissues such as skin and internal organs, the penetration depth of OCT does not exceed a few millimeters due to multiple scattering of light caused by inhomogeneous distributions of refractive indices in the tissue. Because the imaging contrast in OCT is from single backscattering from a scatter, the optical signal decays exponentially as a function of depth in the presence of multiple scatterings.² Beyond the one

transport mean-free path which corresponds to 1 to 2 mm in most biological tissues,³ a single backscattered signal is severely degraded, and multiple scattering becomes dominant, which limits the penetration depth of OCT.

Due to this limited penetration depth in OCT, imaging highly scattering tissues, such as breast and skin tissues, has not been fully explored, whereas retina imaging using OCT in ophthalmology has been extensively investigated.⁴ This limited penetration depth of OCT is unfortunate because OCT has much to offer to various fields in biology/biotechnology/life sciences and medical diagnoses with its unique noninvasive optical sectioning capability, its high spatial resolving power, and its lack of radiation damage. For example, pathological studies in dermatology have shown the potential of OCT,⁵ while the accessible depth is restricted to the epidermis and upper dermis layers.⁶ OCT can also be useful for noninvasive diagnoses of cancers;⁷ however, the imaging depth of OCT is confined to a superficial layer which prevents early cancer detection. Multimodal OCT systems equipped with photoacoustic microscopy have been proposed to provide microvascular imaging at greater depths^{8–10} while morphological information on deep tissue regions, required for the exact understanding of vascular properties, is still inaccessible.

Several approaches have been proposed to suppress multiple light scattering in OCT imaging. Refractive index matching using optical clearing agents can reduce multiple scatterings,¹¹ but it requires a long setting time (~10 min). Adaptive optics approaches have been used to correct the aberration;^{12,13} however, they mainly address aberrations but do not suppress multiple scatterings due to the limited degree of control. Spatial and frequency compounding methods reduce speckle noises caused by multiple scatterings and provide an enhanced signal-to-noise ratio (SNR).^{14,15} However, the penetration depth is yet to be improved in spatial and frequency compounding methods.

Recently, wavefront shaping (WS) techniques have shown potential for enhancing the penetration depth. By controlling the wavefront of an impinging beam, control of the light field transmitted through a turbid media can be achieved through linear coherent relationships between input and transmitted fields, which are described by scattering matrices.^{16–18} WS approaches have been applied to low-coherence interferometry, including selective focusing in optical coherence microscopy;¹⁹ the penetration depth has been enhanced in spectral-domain OCT,^{20,21} called wavefront shaping optical coherence tomography (WS-OCT); imaging deep in turbid media by collective accumulation of single-scattered waves from a time-resolved reflection matrix.²² Exploiting this approach, significant advances have been made in the last few years in enhancing the penetration depth of low-coherence interferometric imaging systems. However, only demonstrations with static phantoms have been reported. Imaging biological tissues *in vivo* with wavefront shaping approaches still remains unexplored in OCT systems mainly because (1) it takes a long time to acquire the information about the scattering matrices and control the wavefront of the impinging beams and (2) the movements in tissues scramble the information of the scattering matrices.

In this study, we report the *in vivo* imaging of a live mouse using WS-OCT and demonstrate enhancements in both the SNR and penetration depth. A digital micromirror device (DMD) was used in a spectral-domain OCT system to control the wavefront of the input beams. Significant enhancements in the SNR and penetration depth were observed for an *ex vivo* chicken

*Address all correspondence to: Yong Jeong, E-mail: yong@kaist.ac.kr; YongKeun Park, E-mail: yk.park@kaist.ac.kr

†These authors contributed equally to this work.

breast, *ex vivo* mouse ear, and *in vivo* mouse tail. Compared to an uncontrolled beam illumination, the image signals were enhanced by a factor of three to seven depending on the types of samples and depth positions.

The concept of WS-OCT is shown in Fig. 1. In conventional OCT, a Gaussian beam impinges onto a sample [Fig. 1(a)]. However, multiple light scattering in the tissue prevents optimal light delivery deep into the tissue. As a result, it prevents the delivery of light to a target depth as well as coherent gating in low-coherence interferometry. When the wavefront of an input beam is controlled and optimized, an optical focus at the target depth can be formed in the presence of multiple light scattering [Fig. 1(b)]. This can also be understood in a time reversal manner; when light is emitted deep inside a turbid medium, it will have a complex wavefront after transmitting through the medium, and when light is impinged in a reverse direction with this complex wavefront, a focus can be generated in the original location. To find the optimized wavefront which enhanced the delivery of light to the target scatterer, for each A-line scan, we measured the reflection responses corresponding to various optical wavefront patterns of impinging beams. Then from the measured reflection responses, the optimal wavefront can be obtained by finding the constructive interference condition.^{20,21} Finally, an illumination with the optimized wavefront is applied to the sample, then a depth-enhanced OCT image is obtained.

The experimental setup is shown in Fig. 1(c). The wavefront shaping method is applied to a spectral-domain OCT system. A DMD (0.7× GA, 23 kHz frame rate, Texas Instruments) is used for the modulation of an incident beam. A reference and a sample beam are coupled through a single mode fiber and then reach a spectrometer consisting of a grating and an InGsAs line

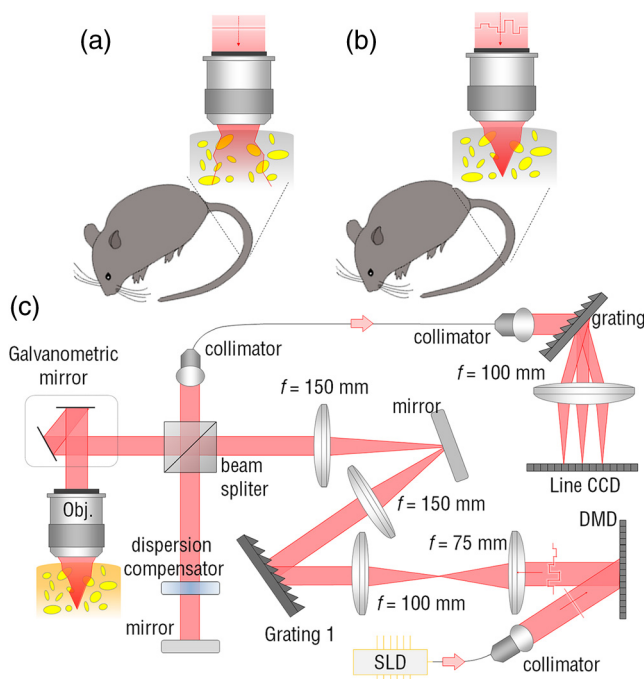


Fig. 1 (a) Inhomogeneous distributions of refractive indices in tissues cause multiple light scatterings, which prevent light delivery to a specific point. (b) By controlling an impinging wavefront, light can be constructively interfered at the target position to allow depth-enhanced OCT imaging. (c) Schematic of the experimental setup.

detector (SU1024-LDH2, 92 kHz frame rate, Sensors Unlimited Inc.). For a single A-scan optimization, input DMD pattern scans, 7500 2-D Hadamard basis, and the corresponding A-scan OCT signals are obtained. The region of interest was set to 200 depth pixels, corresponding to a 580- μm depth range. In parallel, the optimal DMD patterns are calculated for each depth by finding the phase matching conditions from the measured responses. Next, the calculated 200 optimal DMD patterns are sequentially projected to the sample, and the enhanced signals at each depth are compounded to produce a depth-enhanced A-scan image. By scanning over 15 A-scans, a 2-D enhanced image is acquired. The segment size of a pattern was set to 23×23 micropixels in the DMD. The acquisition time for a single A-scan profile is 15 s. The principle of this method is analogous to find a transmission matrix in turbid media,²³⁻²⁷ however, the present method measured coherence- and pinhole-gated reflection responses. The detailed information on the optimization process can be found elsewhere.^{20,21}

Ex vivo chicken breast tissue was imaged with WS-OCT. The superficial layer of sliced chicken tissue was prepared and measured. 2-D images of the tissue obtained with WS-OCT are shown in Fig. 2(a). The reduced scattering coefficient of the chicken tissue was measured to be 0.92 mm^{-1} using an integrating sphere (UPK-100-F, Gigahertz-Optik) based on the inverse adding-doubling method.²⁸ For comparison purposes, the sample was also imaged with the controlled wavefront (Gaussian beam) and the spatial compounding method in Figs. 2(b) and 2(c), respectively. The image with the spatial compounding method was obtained by averaging 25 OCT images recorded with 25 random illumination patterns. The powers of the input beams were set to be the same (0.55 mW) for all three cases. It can clearly be seen that WS-OCT greatly enhances both

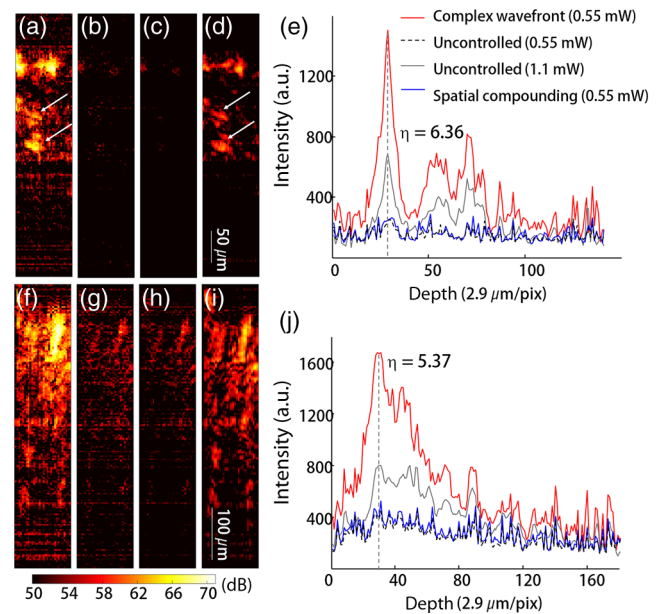


Fig. 2 *In vitro* WS-OCT images of the (a–e) chicken breast and (f–j) mouse ear tissue. (a, f) Optimized image by wavefront control with input power of 0.55 mW. (b, j) Image acquired with an uncontrolled input beam of 0.55 mW. (c, h) Image obtained with the spatial compounding method. (d, i) Image acquired with an uncontrolled input beam of 1.1 mW. (e, j) The averaged A-scan profiles along 15 different A-scans in each case were plotted for the chicken breast and the mouse ear tissue, respectively. The white arrows indicate the additional structures inaccessible with conventional approaches.

the SNR and the penetration depth for *ex vivo* tissue compared with existing methods. In particular, WS-OCT enables the imaging of structures deep inside the tissue that are otherwise inaccessible with conventional approaches [the arrows in Fig. 2(a)].

To validate the tissue structures in the images obtained with WS-OCT, we conducted an experiment for the uncontrolled wavefront with double the incident power at 1.1 mW [Fig. 2(d)]. The structure obtained with WS-OCT with 0.55 mW is comparable to that obtained with the uncontrolled wavefront with 1.1 mW, and this shows that the enhanced signals in WS-OCT resulted from real scatters rather than false artifacts. For a quantitative comparison, the averaged depth profiles over 15 different A-scans in Figs. 2(a)–2(d) are plotted in Fig. 2(e). The enhancement factor η in WS-OCT is defined as the ratio of the signal for the optimized wavefront to that for the uncontrolled wavefront with the same incident power. The enhancement factor at the first layer of the tissue along the green dashed line was 6.36.

Then we imaged the *ex vivo* ear tissue of a mouse. A specific pathogen-free C57BL/6J mouse (Jackson Laboratory) was anesthetized with intraperitoneal injection of a Tiletamine-Zolazepam and Xylazine mixture (30:10 mg/kg body weight), and a piece of an ear was dissected for the imaging shown in Fig. 2(g). All experimental procedures were approved by the Institutional Animal Care and Use Committee of Korea Advanced Institute of Science and Technology. The reduced scattering coefficient of the ear tissue was 0.53 mm^{-1} . The experimental results for the wavefront shaping, the uncontrolled beam, the spatial compounding, and double-powered uncontrolled beam are, respectively, shown in Figs. 2(f)–2(i). Similar to the case with the chicken breast tissue, the wavefront shaping shows an apparently stronger signal and deeper penetration depth compared to existing methods. In Fig. 2(j), the averaged depth profiles over 15 different A-scans are plotted for comparison purposes. An enhancement factor of 5.37 was obtained at the upper layer (indicated as the gray dashed line).

Next, *in vivo* images of a mouse tail were obtained with WS-OCT. A mouse of the same type used in the *ex vivo* study was anesthetized using the same procedures. A photograph of the mouse under imaging and micrographs of a tail section slice of $30 \mu\text{m}$ after hematoxylin and eosin (H&E) stain are shown in Fig. 3(a). Twenty min after the anesthetic injection, three different locations on the distal end of the mouse tail were imaged. The reduced scattering coefficient of the tail tissue was measured as 1.212 mm^{-1} . The experimental results are shown in Fig. 3. For all locations, WS-OCT showed a significantly improved penetration depth and SNR. In particular, multiple-layered structures were visualized with WS-OCT: the double-layered structure at location 1 [Fig. 3(b)] and the triple-layered structures at locations 2 and 3 [Figs. 3(g) and 3(l)] as indicated by gray arrows (note the difference in scales between locations 1, 2, and 3). The shapes and locations of these structures correspond to epidermis, connective tissue textures, and sebaceous glands. However, the uncontrolled beam and the spatial compounding method only visualized the most superficial single layer at all locations. The average depth profiles for 15 A-scans are plotted for each location in Figs. 3(f), 3(k), and 3(q). The enhancement factors for the first layer were 5.26, 6.88, and 6.06 at locations 1, 2, and 3, respectively. These enhancement factors are comparable to that of the former *ex vivo* experiments implying that the efficiency of wavefront shaping is not severely degraded in *in vivo* environments. The enhancement factors at the second peaks were 4.47 for location 1 and 3.97 for location 2, slight smaller than those of the first layers. Notably, the enhancement factor decreases as the depth increases. This may be because the fraction of uncollected light will increase as the depth of the scatters increases. At location 3, although the intensity level of the second peak [Fig. 3(q), the orange arrow] is much smaller than that of the other locations, an enhancement factor of 3.36 is still comparable to the other locations which implies the enhancement does not depend on the absolute level of intensity.

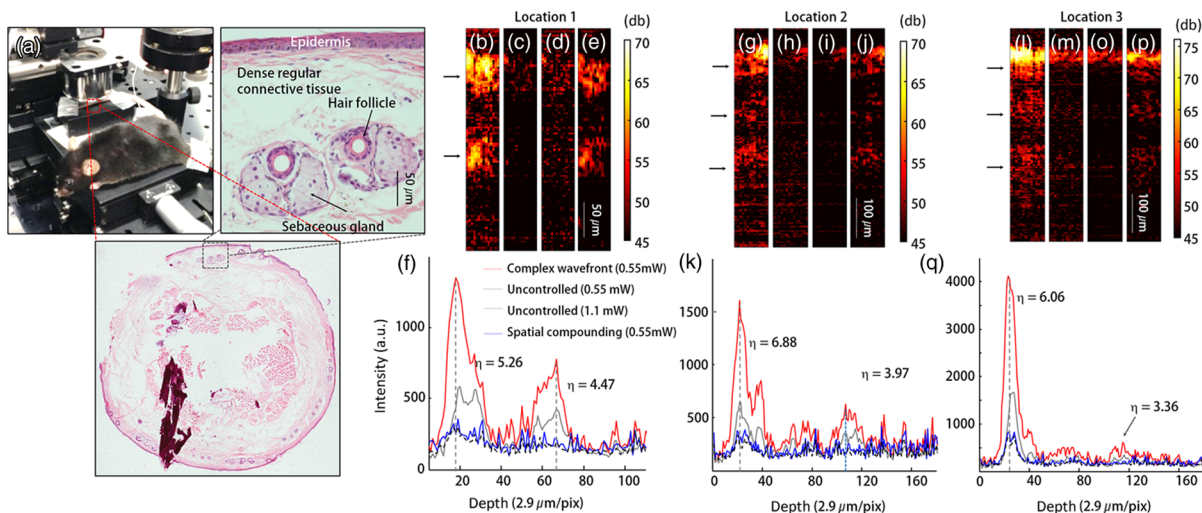


Fig. 3 *In vivo* WS-OCT images of the tissue in a tail of a live mouse. (a) A mouse under imaging and optical micrographs of a tail section slice of $30 \mu\text{m}$, measured with a bright-field microscopy after H&E staining. (b–q) OCT images were acquired at three different locations. (b, g, l) Optimized image by wavefront control with an input power of 0.55 mW. Multilayered structures are indicated as the gray arrows. The shapes and locations of these structures correspond to epidermis, connective tissue textures, and sebaceous glands. (c, h, m) Image acquired with an uncontrolled input beam of 0.55 mW. (d, i, o) Image obtained with the spatial compounding method. (e, j, p) Image acquired with an uncontrolled input beam of 1.1 mW. (f, k, q) The averaged A-scan profiles along 15 different A-scans.

In summary, we present *ex vivo* and *in vivo* tissue images with WS-OCT and demonstrated a significant enhancement in the penetration depth and SNR. For *in vivo* mouse tail imaging, the present approach unraveled the multilayered structures. With WS-OCT, the penetration depth was improved with lower optical power and the results are comparable to the conventional OCT approach at higher power. The signal enhancement factor compared to the uncontrolled input beam reached up to 6.88 at the superficial layer.

This result clearly suggests that wavefront shaping is a promising method of controlling multiple light scattering for *in vivo* imaging of highly turbid tissue. Yet, the current work only demonstrated the imaging of movement-free samples such as mouse tails, due to the slow acquisition speed. Recent studies suggest that the acquisition time must be reduced to the order of a millisecond to overcome the decorrelation time of biological tissues.²⁹ We anticipate that the further improvement of the measurement speed of the present can be accomplished, and this setup will lead to widespread applications of wavefront shaping approaches in OCT. In addition, the depth enhancement presented in this *in vivo* study is still limited within 600 μm , and it is below the usually claimed OCT penetration depth of 1 mm. This absolute depth of penetration can be further enhanced by optimizing the optical elements with an illumination source. Furthermore, the present method can also be expanded to other OCT modalities such as polarization-sensitive or spectroscopic signals, by exploiting large degrees of freedoms in multiple scattering.^{16,30,31}

Acknowledgments

This work was supported by the KAIST, the National Research Foundation of Korea (2015R1A3A2066550, 2014K1A3A1A09063027, 2012-M3C1A1-048860, and 2014M3C1A3052537), and the Innopolis Foundation (A2015DD126).

References

- D. Huang et al., "Optical coherence tomography," *Science* **254**(5035), 1178–1181 (1991).
- A. F. Fercher et al., "Optical coherence tomography—principles and applications," *Rep. Prog. Phys.* **66**(2), 239–303 (2003).
- D. A. Boas, C. Pitris, and N. Ramanujam, *Handbook of Biomedical Optics*, CRC Press, Boca Raton (2011).
- B. E. Bouma et al., "Fourier-domain optical coherence tomography: recent advances toward clinical utility," *Curr. Opin. Biotechnol.* **20**(1), 111–118 (2009).
- J. Welzel et al., "Optical coherence tomography of the human skin," *J. Am. Acad. Dermatol.* **37**(6), 958–963 (1997).
- T. Gambichler, V. Juedicke, and S. Terras, "Optical coherence tomography in dermatology: technical and clinical aspects," *Arch. Dermatol. Res.* **303**(7), 457–473 (2011).
- B. J. Vakoc et al., "Cancer imaging by optical coherence tomography: preclinical progress and clinical potential," *Nat. Rev. Cancer* **12**(5), 363–368 (2012).
- S. Jiao et al., "Simultaneous multimodal imaging with integrated photoacoustic microscopy and optical coherence tomography," *Opt. Lett.* **34**(19), 2961–2963 (2009).
- L. Li et al., "Three-dimensional combined photoacoustic and optical coherence microscopy for *in vivo* microcirculation studies," *Opt. Express* **17**(19), 16450–16455 (2009).
- E. Z. Zhang et al., "Multimodal photoacoustic and optical coherence tomography scanner using an all optical detection scheme for 3D morphological skin imaging," *Biomed. Opt. Express* **2**(8), 2202–2215 (2011).
- V. V. Tuchin and V. Tuchin, *Tissue Optics: Light Scattering Methods and Instruments for Medical Diagnosis*, SPIE Press, Bellingham (2007).
- B. Hermann et al., "Adaptive-optics ultrahigh-resolution optical coherence tomography," *Opt. Lett.* **29**(18), 2142–2144 (2004).
- R. Zawadzki et al., "Adaptive-optics optical coherence tomography for high-resolution and high-speed 3D retinal *in vivo* imaging," *Opt. Express* **13**(21), 8532–8546 (2005).
- N. Iftimia, B. E. Bouma, and G. J. Tearney, "Speckle reduction in optical coherence tomography by 'path length encoded' angular compounding," *J. Biomed. Opt.* **8**(2), 260–263 (2003).
- M. Pircher et al., "Speckle reduction in optical coherence tomography by frequency compounding," *J. Biomed. Opt.* **8**(3), 565–569 (2003).
- A. P. Mosk et al., "Controlling waves in space and time for imaging and focusing in complex media," *Nat. Photonics* **6**(5), 283–292 (2012).
- H. Yu et al., "Recent advances in wavefront shaping techniques for biomedical applications," *Curr. Appl. Phys.* **15**(5), 632–641 (2015).
- I. M. Vellekoop and A. Mosk, "Focusing coherent light through opaque strongly scattering media," *Opt. Lett.* **32**(16), 2309–2311 (2007).
- R. Fiolka, K. Si, and M. Cui, "Complex wavefront corrections for deep tissue focusing using low coherence backscattered light," *Opt. Express* **20**(15), 16532–16543 (2012).
- H. Yu et al., "Depth-enhanced 2-D optical coherence tomography using complex wavefront shaping," *Opt. Express* **22**(7), 7514–7523 (2014).
- J. Jang et al., "Complex wavefront shaping for optimal depth-selective focusing in optical coherence tomography," *Opt. Express* **21**(3), 2890–2902 (2013).
- S. Kang et al., "Imaging deep within a scattering medium using collective accumulation of single-scattered waves," *Nat. Photonics* **9**(4), 253–258 (2015).
- S. M. Popoff et al., "Measuring the transmission matrix in optics: an approach to the study and control of light propagation in disordered media," *Phys. Rev. Lett.* **104**(10), 100601 (2010).
- J. Yoon et al., "Measuring optical transmission matrices by wavefront shaping," *Opt. Express* **23**(8), 10158–10167 (2015).
- H. Yu, J. H. Park, and Y. Park, "Measuring large optical reflection matrices of turbid media," *Opt. Commun.* **352**, 33–38 (2015).
- H. Yu et al., "Measuring large optical transmission matrices of disordered media," *Phys. Rev. Lett.* **111**(15), 153902 (2013).
- J. Yoon et al., "Optogenetic control of cell signaling pathway through scattering skull using wavefront shaping," *Sci. Rep.* **5**, 13289 (2015).
- S. A. Prael, M. J. van Gemert, and A. J. Welch, "Determining the optical properties of turbid media by using the adding-doubling method," *Appl. Opt.* **32**(4), 559–568 (1993).
- M. Cui, E. J. McDowell, and C. H. Yang, "An *in vivo* study of turbidity suppression by optical phase conjugation (TSOPC) on rabbit ear," *Opt. Express* **18**(1), 25–30 (2010).
- J. H. Park et al., "Dynamic active wave plate using random nanoparticles," *Opt. Express* **20**(15), 17010–17016 (2012).
- J. H. Park et al., "Active spectral filtering through turbid media," *Opt. Lett.* **37**(15), 3261–3263 (2012).